Geofluids (2007) 7, 356–368 doi: 10.1111/j.1468-8123.2007.00187.x

Models of iron oxide concretion formation: field, numerical, and laboratory comparisons

M. A. CHAN[1], J. ORMÖ[2], A. J. PARK[3], M. STICH[2], V. SOUZA-EGIPSY[2] AND G. KOMATSU[4]

[1]*Department of Geology & Geophysics, University of Utah, Salt Lake City, UT, USA;* [2]*Centro de Astrobiología (INTA/CSIC), Ctra Torrejón a Ajalvir, Torrejón de Ardoz, Spain;* [3]*Sienna Geodynamics Inc., Bloomington, IN, USA;* [4]*International Research School of Planetary Sciences, Universita' d'Annunzio, Pescara, Italy*

ABSTRACT

Well-exposed Jurassic Navajo Sandstone iron oxide concretions preserve important diagenetic records of groundwater flow and water–rock interactions. Field relationships, precipitation patterns, and geometries of the Navajo concretions provide the basis for input parameters in numerical computer simulations and laboratory chemical bench tests. Although field geometries are very difficult to replicate, numerical simulations and laboratory experiments examine end results such as nucleation and growth of iron oxide concretions, produced from known input parameters. Three numerical simulations show the development of periodic self-organized nucleation centers through Liesegang-type double-diffusion of iron and oxygen. This numerical model simulates a scenario where oxygen is provided by shallow fresh water and iron is sourced from deeper reduced formation water. Concretions form in the region where the two waters interact with each other. Model sensitivities show that advection of water is an important mechanism for supplying the iron, and that acidic conditions in the iron-charged water can cause iron to stay in solution longer to produce nucleation centers that are farther from the input source. Laboratory bench tests with reactions of $FeSO_4$ or $Fe(NO_3)_3$ with KOH show how the precipitation of hydrated iron sulfates or iron-hydroxides may form rinds around an initial, spherical source of iron (i.e. nucleation center). These rinds may show inward growth depending on the concentration of the iron source in relation to the surrounding fluid. A number of complex factors such as concentration and flux, time, and multiple events can create banded patterns during rind growth. Comparisons of the terrestrial examples with numerical and laboratory models have strong implications for understanding similar hematite concretions on Mars.

Key words: concretions, diagenesis, hematite, Mars, Navajo Sandstone, self-organization

Received 11 August 2006; accepted 5 April 2007

Corresponding author: Marjorie A. Chan, Department of Geology & Geophysics, University of Utah, Salt Lake City, UT 84112, USA.
Email: chan@earth.utah.edu. Tel: +1-801-581-7162. Fax: +1-801-581-7065.

Geofluids (2007) 7, 356–368

INTRODUCTION

Concretions are cemented mineral masses that are valuable records of diagenetic, post-depositional changes in sedimentary units because they preserve evidence of groundwater flow and water–rock interactions resulting in mineral dissolution and precipitation. Although sometimes considered geologic oddities, concretions are very common and widespread in sedimentary rocks throughout the geologic record (e.g. Seilacher 2001; Mozley 2003). Concretions are common where groundwater can precipitate cement.

Intensive studies of calcite and siderite concretions have examined their internal zonation and mode of growth (Mozley 1989, 1996; Klein *et al.* 1999; Raiswell & Fisher 2000; Hall *et al.* 2004) and the possible role of microbial influence (e.g. Borkow & Babcock 2003; Mozley & Davis 2005). Calcite and siderite studies show a complex range of macroscopic and microscopic textures that suggest concentric to pervasive growth as well as growth in different hydrologic environments (e.g. Mozley & Davis 2005). Iron oxide concretions are similarly complex and difficult to study. The differences in the abundances of the constituent solutes (Ca and carboxyls in carbonate system are more abundant than Fe and O_2 in water) also suggest there would be significant differences in the reaction-transport mechanisms associated with the two concretion types. Iron oxide concretions result from a series of chemical oxidation and reduction steps, and the nucleation,

precipitation and maturation of polynuclear gels, metastable phases, the role of pH, and stability of different mineralogy are still poorly understood.

Iron oxide (e.g. hematite, goethite) sandstone coloration and concretions are significant indicators of the mobility of iron in groundwater and host rock properties such as porosity and permeability. Iron oxide concretions typically lack any obvious nucleus (Chan *et al.* 2004, 2005) and appear to form in different ways from simple attractive growth around a physical 'seed' nucleus (Mozley 2003). The periodic and dispersed occurrence patterns of the concretions, often pervasive through vast localities, are consistent with chemical self-organization processes (cf. Ortoleva 1984, 1994).

Basic but difficult questions regarding iron oxide concretions are: How do concretions start or nucleate? And what influences their growth? We examine aspects of the concretion forming processes by comparing concretions in the Jurassic Navajo Sandstone of Utah with numerical computer-simulation models of simplified nucleation and laboratory bench-chemical models of concretion development after nucleation. This permits consideration of fluid characteristics that are often difficult to evaluate in ancient rocks, such as the dominant mode of solute transport (diffusion or advection), evolution of fluid composition, rates of fluid flux, and influence of pH, temperature, and timing.

Interest in spheroidal iron oxide concretions has been heightened due to the recent spectacular success of the Mars Exploration Rover Opportunity. Better understanding of the precipitation processes leading to spheroidal iron oxide concretions on Earth may provide insights into the formation of the Mars spherules that have been interpreted to be iron oxide concretions (Chan *et al.* 2004; Ormö *et al.* 2004), popularly referred to as 'blueberries' in the Burns formation (Squyres *et al.* 2004; Grotzinger *et al.* 2005) at Meridiani Planum, Mars. These Mars concretions are hematite (Christensen *et al.* 2004) and preserve information concerning the history of liquid water and, thus, of possible ancient habitats for life on Mars (Squyres & Knoll 2005). Terrestrial analogs for sedimentology, stratigraphy, diagenesis, and geochemistry are extremely important in interpreting the rich new Opportunity data. Although schematic small-scale computer and laboratory models cannot directly replicate either terrestrial or Mars conditions, the model sensitivities illustrate the influence of fluid interactions in concretion growth.

NAVAJO SANDSTONE CONCRETIONS

Iron mobilization and precipitation

The Lower Jurassic Navajo Sandstone of southern Utah contains color variations and diagenetic iron oxide concretion mineralization (Fig. 1) that can be explained in terms of a three-step diagenetic process in a very porous pure quartz arenite involving a range of groundwater flow conditions and multiple fluids. The model can be summarized as: (i) iron sourced from dispersed early diagenetic reddening (Walker 1967, 1975; Berner 1969, 1980), followed by (ii) iron mobilization via bleaching through chemical reduction, and then (iii) final iron oxide precipitation into concentrated concretion masses upon oxidation (where reduced fluids carrying iron meet with oxygenated waters). The model is further detailed and synthesized in several papers (e.g. Chan *et al.* 2000, 2004, 2005, 2006; Beitler *et al.* 2003, 2005; Parry *et al.* 2004), and is consistent with established iron oxide chemistry (e.g. Cornell & Schwertmann 2003).

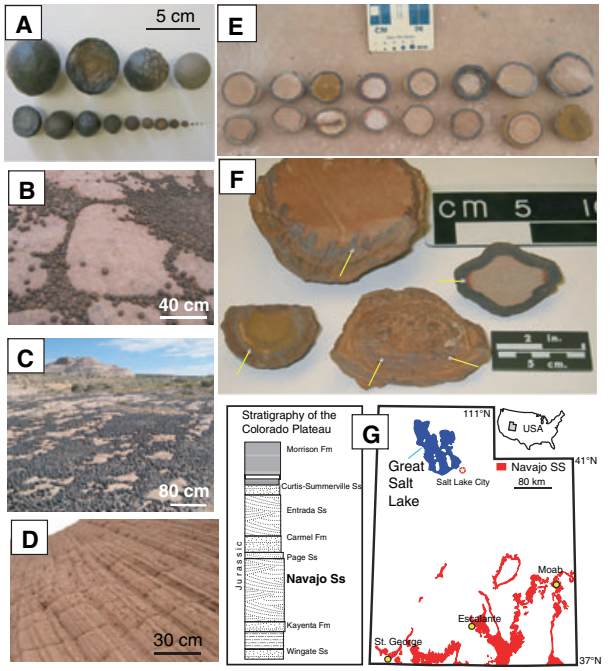

Fig. 1. Jurassic Navajo Sandstone: (A) examples of different sizes of common spherical iron oxide concretions: (B–C) common concretion accumulations, (D) *in situ* concretions, (E) mixed populations of concretions with various rind or internal layer structures, (F) examples of bulbous inward growth projections from large concretion forms, in addition to 'bleeding' and apparent inward diffusion along permeable laminae (shown by arrows) and (G) stratigraphic section and map of Navajo Sandstone exposures in southern Utah.

Concretion forms

The Navajo Sandstone concretions have many shape varieties, but we herein focus on common spheroidal shapes often referred to as 'marbles'. These span a wide range of sizes (mm to cm), and have diverse internal structures (rind, 'onion-layered', and massive/solid). Some Navajo Sandstone reaction fronts show widespread micro- or mini-concretions (analogous to Mars 'microberries' of Squyres

2005) about 1 mm or less in diameter at close spacings of approximately 1 cm or less. The well-sorted quartz arenite provides a relatively simple host rock with little grain reactivity, allowing focus on the iron oxide mineral cement and evaluation of the parameters affecting the cementation process. Concretion cement can be hematite or goethite, and sometimes both.

Large concretions (>5 cm diameter) commonly exhibit internal patterns including rinds, multiple layers, and bulbous growth toward the interior (Fig. 1F). Here we focus on simple forms and what they can tell us, in order to contribute to eventual understanding of large and complex forms.

Concretion chemistry

Formation of concretions requires that reactants reach some level of super-saturation (e.g. nucleation threshold) with respect to equilibrium precipitation. The identity of the reactants differs with the chemical composition of the concretion. Hydrous ferric oxide concretions likely precipitate as a consequence of oxidation of ferrous ion in solution according to the hematite reaction:

$$2Fe^{2+}_{(aq)} + \tfrac{1}{2}O_{2(g)} + 2H_2O_{(l)} = Fe_2O_{3(s)} + 4H^{+}_{(aq)} \quad (1)$$

Or the goethite reaction:

$$2Fe^{2+}_{(aq)} + \tfrac{1}{2}O_{2(g)} + 3H_2O_{(l)} = 2FeO(OH)_{(s)} + 4H^{+}_{(aq)} \quad (2)$$

Reactants are $Fe^{2+}_{(aq)}$, $O_{2(aq)}$, and $H^{+}_{(aq)}$. The effective free energy difference between goethite and hematite is very small (Wolery *et al.* 1990; Stumm & Morgan 1996). Thus, formation of hematite, goethite, or hydrous ferric oxide can be a consequence of subtle differences in conditions such as pH, Eh, $O_{2(aq)}$, or other factors. Hematite may result from maturation of goethite by dehydration:

$$2FeO(OH)_{(s)} = Fe_2O_{3(s)} + H_2O_{(l)} \quad (3)$$

Furthermore, ferrihydrite can also transform into hematite. As ferrihydrite requires significantly lower temperatures than goethite to transform to hematite, it may be a promising model for hematite formation under near-surface conditions (Schwertmann *et al.* 2004).

Other porous Mesozoic sandstone units on the Colorado Plateau show iron sulfide concretions (e.g. Thorson & MacIntyre 2005) that may reflect slightly different chemistries and diagenetic conditions than the Navajo Sandstone. In more reducing and sulfur rich conditions, early iron sulfide concretions can precipitate by uniting ferrous ion and reduced sulfur in an oxidation–reduction reaction:

$$2H_2S_{(g)} + \tfrac{1}{2}O_{2(g)} + Fe^{2+}_{(aq)} = FeS_{2(s)} + H_2O_{(l)} + 2H^{+}_{(aq)} \quad (4)$$

The $H_2S_{(g)}$ in the reaction likely results from chemical reduction of aqueous $SO^{2-}_{4(aq)}$, and the $S^{2-}_{2(aq)}$ in pyrite may result from reduction of aqueous $SO^{2-}_{4(aq)}$ or from oxidation of $H_2S_{(s)}$ as shown in the reaction (see Williamson & Rimstidt 1994 for a review of pyrite oxidation). It is unlikely that all reactants are in one solution. Therefore, at least two solutions are likely involved: one carrying oxidized species and one carrying reduced species, or one containing reduced S and one containing the $Fe^{2+}_{(aq)}$.

The rocks that host concretions may contain a diverse assemblage of potential mineral and nonmineral nuclei such as clay minerals, feldspar, carbonate cements, organic debris, and bacteria. Typically a nucleus is not visible in thin or polished section, and it is generally difficult to distinguish structure in the small and abundant 'mini' or 'microberry' sizes. However, it is possible that any nucleus may have been consumed in chemical reactions. In some cases there is different iron oxide coloration in the center of some concretions that may be a partial remnant nucleus. Surface kinetics may also control the rate at which dissolved species interact with the mineral precipitate, and it is possible that there is a microbial microenvironment that controls (e.g. enhances) precipitation, even if there is not a normal thermodynamic equilibrium with the physiochemical ambient conditions.

In this study, we assume that concretion cementation via a population of nuclei occurs once the water composition exceeds a certain nucleation threshold (e.g. Ortoleva 1994). Spacings between concretions are determined by the spacings between the locations in sediments where the relevant pore-water concentration reaches the nucleation threshold of hematite. Reaction rates, mass-transfer processes, and sediment heterogeneity interact to produce nonhomogeneous distribution of solutes. Once a nucleation threshold has been reached, growth of a concretion is controlled predominantly by reactant supply and the concretion precipitation rates.

The net effect of the interaction between multiple solutions, supply rates of reactants, rate of precipitation, and nucleation leads to a diversity in size, shape, spacing, mineralogy, and other characteristics of concretions. If nucleation takes place at two nearby sites and reactant supply is abundant, joined forms or doublets might result. Similarly, when multiple closely spaced nucleation sites are present and reactant supply is limited, many closely spaced but small concretions might result. Inward growth from mass transfer by diffusion is evident from field examples (i.e. bulbous growth, Fig. 1F), as well as in observations of cut concretions showing interior structure (Souza-Egipsy *et al.* 2006). An additional complication is migration of the reaction front boundary that separates the two solutions. If a reaction front traverses the same sediment repeatedly, complex dissolution and precipitation episodes can occur, potentially producing leaching and/or laminated precipitation layers and other complex textural and morphological features.

METHODS

Numerical computer simulations

Understanding the evolution of internal structures can contribute significantly toward understanding the diagenetic environment where concretions formed. Our approach to the structures in the Utah concretions examines two stages: early precipitation of unstable Fe-hydroxide analyzed with a computerized numerical simulation technique (see Appendix), followed by a 'ripening' or recrystallization of the unstable hydroxides into more stable iron oxides analyzed by *in vitro* precipitation experiments. Formation of discretely spaced early mineralization centers or concretions is demonstrated through numerical experiments that effectively simulate Liesegang banding phenomena involving Fe and oxygen cross-diffusion (Park & Ortoleva 2003; Park *et al.* 2005).

Model parameters

Liesegang bands evolve when solutes required for precipitating a mineral are introduced from two opposite ends of a hosting medium. Liesegang banding (2-D features of 3-D surfaces) is a 1-D feature in the direction perpendicular to the surfaces of the bands, and occurs in relatively homogeneous hosting media (Flicker & Ross 1974; Fu *et al.* 1994; Henisch 2005). For simple Liesegang bands to form, therefore, chemical reactions occur in 1-D systems that lack textural or compositional variation in the direction perpendicular to the direction of solute migration, such that the solute migration front is not perturbed by the medium's chemical and textural heterogeneity (Crank 1979).

In geologic systems with complex 2-D and 3-D compositional and textural heterogeneities, it is possible for the textural heterogeneity to perturb the smooth diffusion front and produce nonplanar, i.e. spotty, precipitation patterns and possibly nucleation centers. For instance, diffusive flux is typically expressed as a function of potential chemical gradient of a solute multiplied by a porosity factor (Crank 1979; Boudreau 1996). In highly heterogeneous 2-D and 3-D systems, chemical fronts may become nonplanar because of the solute diffusivity differences produced by porosity variations. Similar mechanisms have been observed in chemical wave systems of porous and nonporous media. Typically, diffusive transport mechanisms with 2-D and 3-D heterogeneities produce regularly spaced speckled patterns (e.g. see Scott & Showalter 1992, and Roussel & Roussel 2004 for more theoretical discussions).

Simulations

In this study, a 1-D Liesegang numerical water–rock interaction model is used as a first approximation to characterize the spacing between concretions. The heterogeneous geological and geochemical conditions that could give rise to the concretions formed in the Jurassic sandstones of Utah are obviously much more complex. The 1-D model is based on solving a set of continuity equations and equilibrium reaction expressions in a finite difference framework (see Appendix). For the series of 1-D simulations here, waters of fixed compositions were imposed at both ends of the model in order to induce diffusive influx of iron- and oxygen-charged waters into the sediments. Table 1 shows simulation configuration and geological and geochemical assumptions used in the simulations. The conditions imposed are our estimates of the geochemical conditions and environment that the concretions formed in. A number of the parameters were selected for ease of data manipulation. Two parameters that require further elaboration are the reaction rate coefficient of hematite and the nucleation threshold. Because there are few data on the hematite precipitation rate, the rate coefficient was approximated by multiplying calcite reaction rate coefficient (e.g. Sjoberg & Rickard 1984) by a factor of 100, to allow faster hematite precipitation compared with calcite. This is a reasonable approach, because the simulations are used to test the distribution pattern of hematite nucleation, and not the total amount of hematite precipitating over geologic time. Nucleation threshold values are also unavailable in the literature. The value of 1.5 used in the simulations is based on the assumption that hematite would require a significantly greater nucleation threshold value than typical carbonate or silicate minerals. If a lower value is used, the spacing between the precipitates becomes shorter.

The simulations are run over a distance of 1 m. The sediment is assumed to consist only of spherical quartz

Table 1 Numerical parameters for computer simulation program Sym.8.

Parameters	
(1) Temperature	64°C
(2) Hematite reaction rate coefficient	5.95×10^{-15} moles cm^{-2} sec^{-1}
(3) Equilibrium constant	1.9×10^{-66}
(4) Nucleation threshold	1.5
(5) Solute diffusion coefficient (cm^2 sec^{-1})	
H^+	1.4×10^{-5}
OH^-	9.0×10^{-6}
Fe^{2+}	1.2×10^{-6}
$O_{2(g)}$	5.4×10^{-6}
Concentrations	
(6) $[H^+]$	1.0×10^{-6} M (= pH 6)
(7) $[Fe^{2+}]$	4.0×10^{-15} M
(8) Fugacity $O_{2(g)}$, $f(O_{2(g)})$	5.0×10^{-14}

Assumptions for parameters in Table 1: (1) Diagenetic temperature (<100°C) estimated from burial depth of Jurassic Navajo Sandstone (Chan *et al.* 2004). (2) Approximation; 100 times calcite reaction rate constant (also see text discussion). (3) Thermodynamic database, EQ3/6 software package (Wolery *et al.* 1990). (4) Approximation; see text for discussion. (5) Boudreau (1996). (6) & (8) Typical groundwater values (Stumm & Morgan 1996). (7) Approximated by equilibrating hematite at 100°C, pH 5, and $f(O_{2(g)})$ 1.0×10^{-20}.

grains. Chemical compositions of waters should emulate the natural conditions; however, the exact values for ancient waters are unknown, so simulated water compositions (Table 1) are approximations. The simulations test the sensitivity of concretion spacing to advection rate and the composition of the iron-charged water.

In the simulations, Fe^{2+}-charged water is introduced at the left boundary of the model. $O_{2(g)}$-charged water is simultaneously introduced at the right-side boundary. Lower concentration of Fe^{2+} than $O_{2(g)}$ is assumed, so formation of hematite in this system is controlled by the supply rate of iron. Precipitation occurs when the saturation of the water with respect to hematite reaches the nucleation threshold. Once the nucleates form, hematite saturation becomes suppressed in the immediate vicinity of nucleates as the nucleates consume the nearby solutes. Simulations show that oxygen can effectively migrate upstream as long as the advection rate is slower than the diffusive flux rate of the solutes (i.e. a water advection rate <5 cm $year^{-1}$ for this simulation).

Laboratory experiments

The numerical simulations explain the sequence of processes leading to the 2-D and 3-D self-organized nucleation centers (e.g. Ortoleva 1984, 1994) where the first precipitates form as spherical, amorphous nodules of iron-hydroxide. It is not clear how these amorphous nodules develop into the solid spherical concretions observed in the Navajo Sandstone. To investigate the continuous process of the iron oxide concretion growth, we performed controlled laboratory experiments aimed at analyzing the further development of the iron-hydroxide nodules from the first stage of our study (i.e. numerical simulation). We studied two different chemical reactions in two different physical environments: (i) the reaction between $FeSO_4$ (1 M) and KOH (1 M) solutions where sand was used as the host environment, and (ii) the reaction between $Fe(NO_3)_3$ (0.1 M and 0.05 M) and KOH solutions (0.1 and 0.05 M) in a physical host environment of 1-D agarose (a standard, neutral gel framework for chemical bench tests, as described further in the section on agarose experiments).

On the small scale and short time frames feasible within a laboratory, it is extremely difficult to directly reproduce the formation of nucleation centers for spherical iron-hydroxide precipitation. Instead, the experiments rely on forced nucleation (adding chemical reactants together) to try to simulate how iron precipitates when the first stage of reactions is created by a strong pH gradient of different chemicals. For simplicity, experiments were done in two dimensions.

Sand experiments

A thin film of fine- to medium-grained sand (grain size approximately 0.6 mm) comprising a thickness of a few sand grains was spread on the bottom of a Petri dish to serve as host sediment for the mixing of two fluids ($FeSO_4$ 1 M solution and KOH 1 M solution). The sand was autoclaved for sterilization. In the first experiment, the sand was soaked with $FeSO_4$. Then KOH was dropped (about 2 drops per second, 400 μl total) on one spot of the $FeSO_4$ soaked sand. In the second experiment, the same volume of $FeSO_4$ solution was dropped on sand soaked with KOH solution. In a third experiment, the sand in the central part of the dish was soaked with KOH solution and, simultaneously, the sand in the periphery with $FeSO_4$ solution. This caused the two fluids to meet and react in a circular perimeter in the sand.

Agarose experiments

Experimental studies of precipitation reactions are routinely performed in agarose gel systems (e.g. Müller & Ross 2003). These have an advantage over other porous media in that they provide an experimental environment that allows diffusive transport of small molecules, reaction, and fixation of the precipitate at the location of the gel matrix where precipitation occurs. Gel systems also provide convenient visual inspection of the reaction and allow mechanical handling and further analysis of the medium after precipitation has occurred. The experiments were performed under room conditions in sterile Petri dishes. The reaction between $Fe(NO_3)_3$ and KOH forms ferrihydrite (Cornell & Schwertmann 2003), which is of chemical interest because it may be a precursor to the iron oxides observed in both Utah marbles and the Meridiani 'blueberry' concretions, though in those cases there were most likely other reactants.

The reactant-impregnated agarose gels were created by first dissolving 40 g $Fe(NO_3)_3{\cdot}9H_2O$ or 28 g of KOH in 500 ml distilled water preheated to 90°C (Schwertmann & Cornell 2000). The final concentrations used were 0.1 and 0.05 M in several combinations (see Table 2). By using gels made with different concentrations of reactants, we attempt to distinguish the movement of the reaction front as a function of the concentration and the deposition of the precipitates with time.

The solutions were mixed with the agarose so that the agarose concentration was 1.5% in all experiments. However, only the agarose made with KOH produced a final gel hard enough to allow a circular hole to be cut out in

Table 2 Chemical concentrations used for both outside and inside agarose configurations in laboratory bench tests (Figs 4 and 5).

KOH (M)	$Fe(NO_3)_3$ (M)
0.1	0.1
0.05	0.1
0.1	0.05
0.05	0.05

the center of the dish. The agarose made with the $Fe(NO_3)_3$ has a very low pH (2) that inhibited the agarose hardening. After several hours of cooling, a circular hole was cut in the resulting KOH-containing agarose gel with a plastic cylinder and 25 ml of the Fe-containing agarose/reactant solution was poured into the empty space. The cut-out circular disk of KOH-containing gel was placed in the center of another Petri dish. Fe-containing agarose was then poured around the KOH-agarose gel disk. In this way different combinations with interior and exterior fluids in direct contact with each other could be tested. The results were documented after 9 and 48 h.

RESULTS

Precipitation at a redox front: results from numerical simulations

Three different numerical simulations show how precipitation patterns at a redox front depend on input parameters and boundary conditions. Although the simulations do not show how different sizes of concretions form, field studies show a relationship between size and spacing (e.g. Chan *et al.* 2004). Concretions that are closely spaced tend to be smaller, whereas larger concretions are spaced farther apart. The simulations demonstrate the sensitivity of the concretion spacing to various parameters.

The 1-D Liesegang-type reaction–diffusion precipitation pattern is considered first (Fig. 2A). For the 1 m-long system, the saturation of hematite is initially near zero due to low concentrations of the solutes (Fig. 2A.1). As solutes diffuse inward from both ends, saturation of hematite begins to increase locally. As concentrations of both solutes continue to increase, the saturation reaches the equilibrium value (Fig. 2A.2) and then the nucleation threshold. When saturation reaches the nucleation point, precipitation occurs. Mineral precipitation continues as long as the solution is supersaturated (Fig. 2A.3). As the precipitation at the nucleation point continues, saturation in the immediate vicinity of the precipitates decreases, and solutes in the region diffuse toward the precipitate along the induced solute concentration gradients. Such nucleation points occur in periodic distribution patterns (Fig. 2A.3–A.5) in a system subject to reaction–diffusion processes. The saturation evolution profiles (Fig. 2A) and patterned precipitates have been documented elsewhere in the literature (e.g. Flicker & Ross 1974; Crank 1979; Ortoleva 1994). The periodicity of the nucleation points depends on such factors as nucleation threshold and supply rates of solutes.

The first simulation of a 1-D Liesegang model (Fig. 2B) is limited to diffusive mass-transfer process only (no water influx). In the absence of an influx of Fe-charged water, a few nucleations (approximately 3) occur close to the Fe-charged boundary, mostly within 21–28 days. In Navajo Sandstone outcrops, bands of iron oxide precipitate layers commonly line fractures in sandstones. The spacing and frequency of these layers is consistent with the simulation-predicted values, and is presumably driven by diffusion from Fe-charged waters moving along the fractures.

In the second simulation, an advection rate of 2.5 cm $year^{-1}$ is induced at the left boundary, allowing more iron to be imported into the system (Fig. 2C). This model produces more nucleates (approximately 6) that are farther away from the left boundary.

In the third simulation, sensitivity of the water composition to pH is demonstrated (Fig. 2D). Lower pH water allows a greater amount of Fe^{2+} to stay in solution (see Eqn 1). As this more acidic water mixes with the oxygenated water away from the inlet point, pH increases. The immediate result is that the first nucleation occurs further from the inlet point. It occurs on the order of 250–265 days.

The distribution of and spacing between nucleation centers are functions of the influx rate of solutes (both Fe^{2+} and $O_{2(g)}$) and mineral reaction rates. The lower the pH, the longer iron can stay in solution and thus move farther away from the inlet source. In nature, the heterogeneity of sediments, which can affect the nucleation threshold of

Fig. 2. Numerical simulations of hematite formation resulting from influx of $Fe^{2+}_{(aq)}$ and $O_{2(aq)}$ species from opposite boundaries. Three different simulations were carried out using the same sediment domain configuration (1 m long, quartzose matrix), with changing solute concentration boundary conditions (see Table 1). Periodic distribution of nucleation points occur due to the interaction of the solutes infiltrating inward from both ends. Left = inlet upstream side, where $Fe^{2+}_{(aq)}$ is introduced. (A) Saturation evolution profiles for Simulation 1 show increasing hematite saturation as $Fe^{2+}_{(aq)}$ and $O_{2(aq)}$ concentrations increase (1) toward nucleation threshold (2) and drop down to saturation as precipitation commences (3). Additional nucleation/precipitation occurs in this simulation as solute diffusion continues (4 and 5). Water immediately surrounding the precipitates remains above saturation but loses solutes to the precipitates through a sharp local chemical concentration gradient. (B) Simulation 1 with diffusion only. Both $Fe^{2+}_{(aq)}$ and $O_{2(aq)}$ concentrations increase as diffusive infiltration of solutes progress (see text for discussion). Saturation value of 1 is when water is at equilibrium with hematite. Nucleation of early hematite occurs near the left border. Inverted triangles show where nucleation occurred due to the increasing local solute concentrations. Diffusion produces nucleations close to the iron input source (left). (C) Simulation 2 with slow advection (2.6 cm $year^{-1}$) of $Fe^{2+}_{(aq)}$-charged water produces more widely dispersed nucleation. Advection introduces a greater amount of iron and creates iron oxide precipitation farther from the Fe source at left. (D) Simulation 3 combines diffusion, advection, and a lower pH of the Fe-rich water, allowing the Fe to stay in solution longer and to be moved farther from the input source. (E) Schematic diagrams of outcrop patterns for the Simulations 1, 2, and 3. Diffusion-only system (Sim. 1) results in hematite bands immediately adjacent to the fracture, whereas diffusion combined with advection results in distributed precipitates (Sim. 2 and 3) in the main body of the sandstone. Changing water composition, in this case pH of the infiltrating Fe-rich water, allows precipitates to form farther away from the inlet (Sim. 3) and also results in larger concretions.

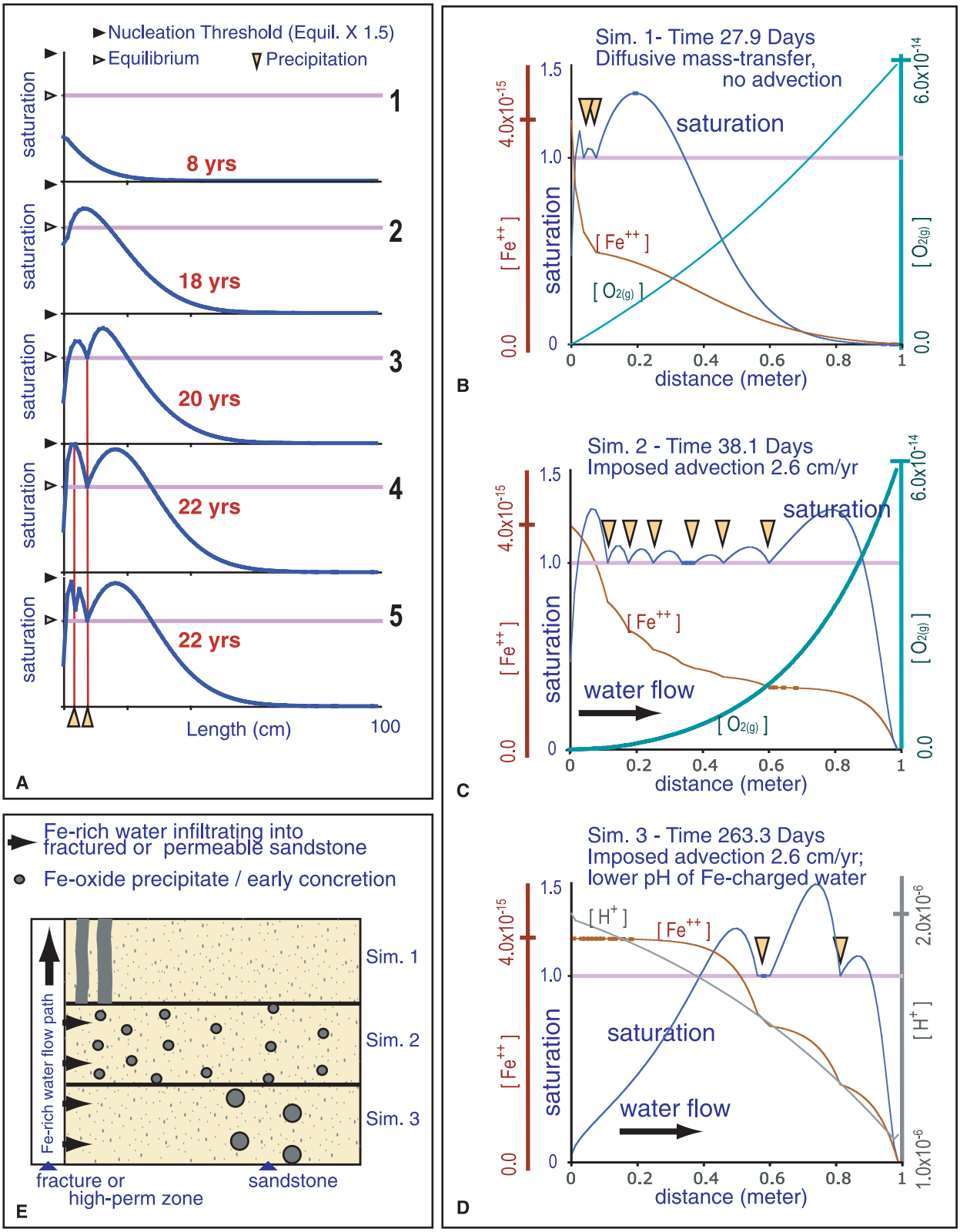

minerals as well as the diffusion of solutes, also has an important role in determining the distribution of the nucleation centers. The Fe-hydroxide nodules may undergo further reactions as the pore water chemistry changes, due in part to slow silicate mineral diagenesis reactions as well as influx of meteoric or other aquifer

waters. Secondary processes that contribute to the evolution of structured internal morphologies of concretions are emulated in the laboratory results discussed below. The reaction rates of natural minerals are slow, and the laboratory experiments demonstrate what can be learned from forced chemical reactions.

Laboratory iron precipitates: sand host

Immediate interaction of injected KOH fluid with soaked $FeSO_4$ substrate first forms a greenish, amorphous, hydrated iron sulfate precipitate at the chemical interface (Fig. 3A). The injected fluid continues to spread until, suddenly, a more distinct, soft rind forms (Fig. 3B) that reddens due to the changing pH. The rind formation halts further spread of the fluid. In experiments 1 and 2 (see 'Sand experiments' above), the rind of the 'concretion' grows inwards, regardless of whether the experiment is done with the iron solution mainly outside or inside of the rind. The rind growth stops after a few hours, possibly because the rind separates the two reactants. Dropping new iron-solution inside a 'concretion' in experiment 1 showed that the KOH solution inside still had capacity to react (i.e. not all reactants had been consumed). The precipitation of hydrated iron sulfate continues, driven by the increasing pH, and after 15 min the greenish rind becomes red and harder (Fig. 3C). The resulting red precipitate is identified as rozenite ($FeSO_4{\cdot}7H_2O$) by XRD. After 48 h, all the green precipitate had turned red, and after 72 h no further change was observed. The concretions from $FeSO_4$ injected into KOH formed more distinct rinds, apparently due to the fact that the $FeSO_4$ does not spread outward as fast as the KOH solution, and thus forms a concentrated pool when the initial rind forms. During this process, Fe ions from the iron source of the interior of the 'concretion' seem to diffuse toward the rind, causing inward growth. As precipitation proceeded, the interior became depleted in green iron precipitate and the sand again became more visible. The third experiment also generated a rind, but the interior of the 'concretion' lacked green iron precipitate. In this case the rind also grew inwards.

After several hours, a breach of the rind occurred in one of the 'concretions' of experiment 3 due to a slight shaking of the Petri dish. Some of the exterior solution ($FeSO_4$) passed through the rind and formed new precipitate in the form of new rinds of rozenite (Fig. 3C). This result hints at one possible cause for the formation of 'onion layered' concretions: cracking of the outer rind (for example during dehydration), and later advective re-introduction of more reactants. Such banding might also be caused by Liesegang-type diffusion due to a chemical (e.g. pH) gradient (see below).

Laboratory iron precipitates: agarose host

The agarose experiment allows a more detailed view of diffusion and precipitation than the sand experiment, with its larger pore-space and irregular grain surfaces. In all agarose experiments, the reaction had caused a darker brown-reddish color at the contact area after 9 h (Fig. 4A–H). In the cases where the KOH gel was placed in the center, the precipitation occurred in this central area (Fig. 4A–D). In the cases where the $Fe(NO_3)_3$ agarose was placed in the center, the iron solution diffused outward into the KOH-gel, so that the inner circular space was depleted of iron and a distinct rind formed in the KOH gel (Fig. 4E–H). In some of the cases with KOH in the center the precipitated iron-hydroxide began to disappear after 48 h (compare Fig. 4A,B with Fig. 5A,B). This was most obvious when the outside iron concentration was highest (Fig. 5C,D). The rinds became thick and permanent only when the source of iron was surrounded by the KOH fluid (Fig. 5E–H).

When the iron concentration of the inside gel was greater than or equal to the outside KOH concentration, the rind became thicker and denser (Fig. 5E,G,H). When the KOH concentration outside was lower than the iron concentration inside, diffusion went farther from the

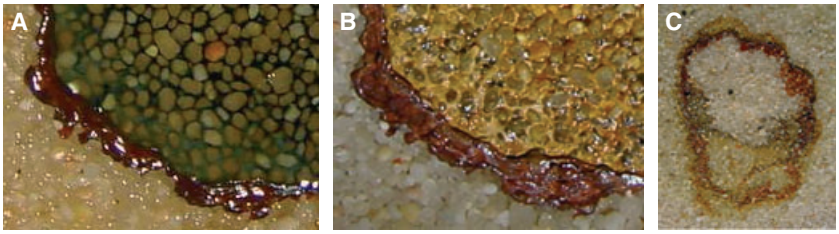

Fig. 3. Bench tests with extreme chemical solutions produce immediate formation of iron precipitates. (A) An initial distinct, soft, greenish 'nodule' forms. Its rind turns red as pH increases. This rind grows inwards, possibly due to diffusion of iron within the 'nodule'. (B) Rind growth stops after a few hours, possibly because the rind becomes less permeable and separates the reactants. Frame A is 15 min and Frame B is 72 h after first reaction. Frame width approximately 12 mm. (C) Laboratory 'concretion' with possible preliminary stage of 'onion layering' due to secondary rind formation after outside fluids enter through breaches in the first rind. Frame width is 3 cm.

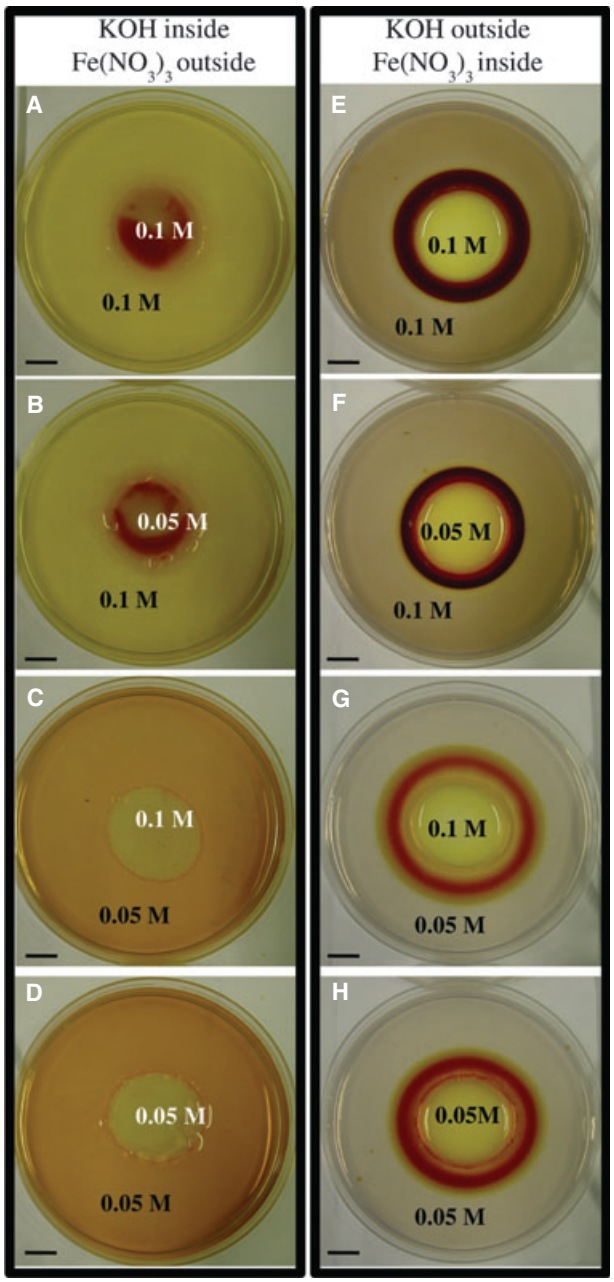

Fig. 4. Laboratory experiments involving 1.5% agarose with KOH and $Fe(NO_3)_3$ solutions after 9 h. (A–D) Disks of KOH–gel of different concentrations inside a liquid agarose solution of $Fe(NO_3)_3$. (E–H) $Fe(NO_3)_3$ solution filling a central hole in KOH-gels of different concentrations. A rind is formed in the KOH gel in contact with the liquid iron-containing agarose, which then diffuses into the KOH gel. Bar = 1 cm.

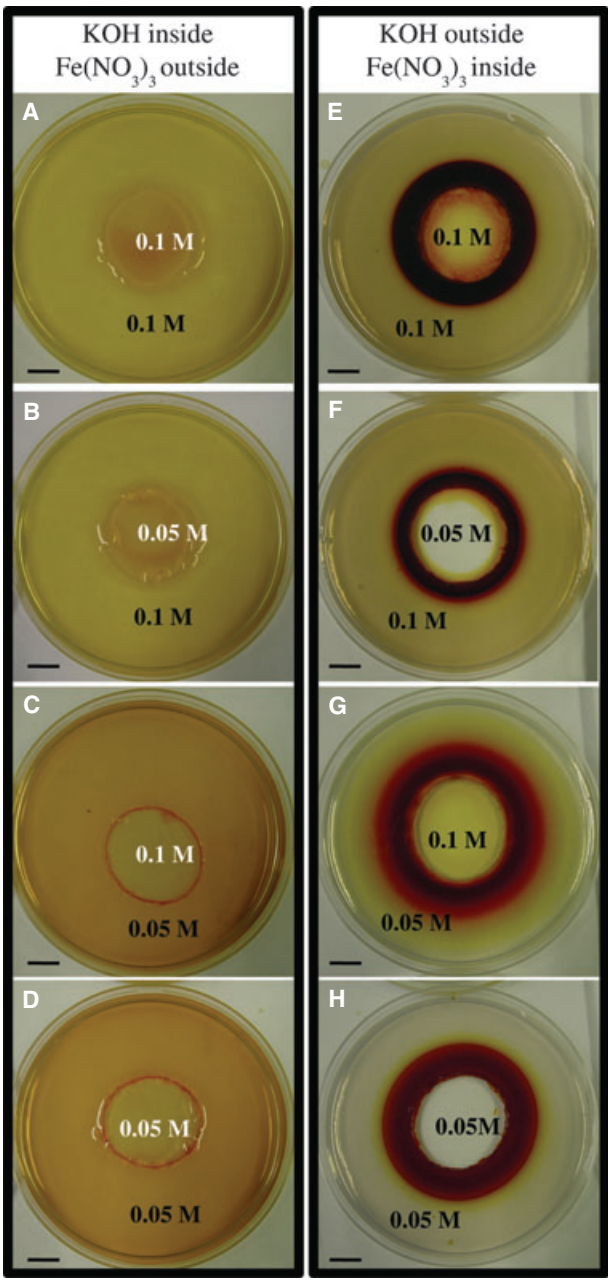

Fig. 5. Conditions after 48 h of the experiment displayed in Fig. 4. In the cases with KOH inside the precipitation is relatively weak (C, D) and may even disappear with time (A, B). Only the rinds formed by diffusion of iron ions into the surrounding KOH-gel become thick and dense (E–H). In E, G, and H the rind also thickened inwards. The absence of inward thickening in F may be due to the relatively low iron concentration in the interior. Bar = 1 cm.

source area (Fig. 5G). When the KOH concentration outside was higher than the iron concentration inside, the iron-hydroxide precipitation rind moved a shorter distance (Fig. 5F). When the inside and the outside concentrations were low and the same, the rind proceeded as far as with the higher concentrations, but became somewhat less dense (Fig. 5H).

The iron-hydroxide precipitation front moves into the KOH solution. Behind the diffusive front the rind thickens toward the source of iron (Fig. 5E,G,H). Thus, in the only combination of fluids that produced a permanent precipitate (i.e. iron source as interior fluid), there was outward diffusion of iron ions. We assume that the resulting pH

gradient generates a zone behind the diffusion front that causes the rind to thicken inwards. In general, the experimental rinds showed banding, i.e. rinds were inhomogeneous or showed abrupt changes of color.

DISCUSSION

Both the numerical models and the laboratory experiments show sensitivity to certain variables and their potential effect on the formation of iron oxide concretions. Examination of numerous iron-oxide concretions (Chan *et al.* 2000, 2004, 2005; Beitler *et al.* 2005) reveals a general lack of any macro nucleus, although it is difficult to assess whether the nucleation centers have been subsequently consumed during growth of the concretions. The numerical simulation models suggest that nucleation of the earliest precipitates, and their spacing, may depend on the supply of solutes. An Fe-rich water flowing at a modest rate, and the reaction–diffusion mechanism, can generate regularly spaced nucleation and precipitation.

In the numerical experiments, concretions form when two waters (reduced formation water and fresh ground water) carrying two necessary solutes (Fe^{2+} and $O_{2(g)}$, respectively) come in close proximity. The waters can, but are not required to physically mix. Oxygen can diffuse into the Fe-rich water to create the super-saturation condition necessary for hematite precipitation. If the waters were stagnant, this system would become equivalent to a Liesegang-type reaction–diffusion system, where only limited precipitation occurs (Fig. 2B). However, if the reduced Fe-rich water moves slowly through the medium, and if the fresh ground water can provide a continuous supply of oxygen, then significant amounts of hematite can be precipitated in the sandstone host (Fig. 2C–E). The periodic, or self-organized patterning of the hematite precipitates in sandstone is also a result of the two waters exchanging solutes (with or without physically mixing).

Some concretions clearly show bulbous inward projections (Fig. 1F), suggesting some inward growth, perhaps limited by the amount of available reactants or the low-permeability seal the rind eventually constitutes. Scanning electron microscope ultrastructural studies of the iron-oxide rind of a Navajo Sandstone concretion by Souza-Egipsy *et al.* (2006) show an inward increase in hematite crystal size, from almost amorphous at the outer perimeter to micro-crystalline toward the center. This may indicate an initially rapid, but progressively slower (i.e. starved) precipitation.

It is also possible that the diffusion occurring within the amorphous iron-hydroxide 'nodule' during inward rind growth can generate spherical, concentric zones through the same process as Liesegang banding. This phenomenon was not observed in the sand experiments, although distinct banding occurs within the rinds of the agarose experiment.

It is difficult to evaluate the exact or absolute timing of concretion cement precipitation in the Navajo Sandstone marbles as there is little material that can be radiometrically dated (Chan *et al.* 2001). Growth can happen quickly given the proper conditions (Berner 1968), and it is also clear that reactions can happen faster and easier at higher temperatures (e.g. Morris *et al.* 2005).

Variations in the Navajo concretion forms are likely due to more complicated processes working over geologic time, perhaps episodically, in an open geologic setting that cannot be easily replicated in a laboratory model. Furthermore, there may be biogenic parameters (e.g. Chan *et al.* 2006; Souza-Egipsy *et al.* 2006) that can enhance geological processes, as well as kinetic and scaling issues that cannot be evaluated here. The laboratory experiments nevertheless provide a baseline for comparison and examining cause and effect of different processes (i.e. nucleation and growth).

The laboratory experiments represent a stage of concretion formation after generation of early nucleation points in the sediment. In order to rapidly simulate the formation of spherical iron precipitates, we used seeding and extreme chemical solutions in a 2-D experimental setting (forced precipitation). The laboratory method followed in this study resulted in the formation of hydrated iron sulfates (sand experiment) and ferrihydrite (agarose experiment). Ferrihydrite is the initial precipitate that results from rapid hydrolysis of Fe^{3+} solutions. This precipitate transforms to goethite and/or hematite if stored underwater, even at ambient temperature (Schwertmann & Cornell 2000). Although the circular shape of the laboratory 'concretions' is not due to the process of self-organization and diffusion expected in the field, the experiments may, nevertheless, provide a simple model showing the importance of chemical reactivity, and the transition from amorphous spheres into solid concretions. The experiments do show that variations in the amount of reactant, and the ability to seal off the fluids (and not allow more reactants in) may be controlling factors in how concretions grow, and suggest a mechanism for producing rinds, layering, or solid interiors.

Implications for Mars

The first terrestrial analog studies related to the Mars hematite spherules suggested that the presence of concretions on Mars implied groundwater flow and certain host rock parameters (Chan *et al.* 2004; Ormö *et al.* 2004). Micro concretions (approximately 1 mm or smaller) and small 'blueberries' (approximately 4.3 mm diameter) were discovered in the Opportunity Rover explorations of Meridiani Planum (Herkenhoff *et al.* 2004; Squyres *et al.* 2004; Squyres 2005). In the context of the modeling presented

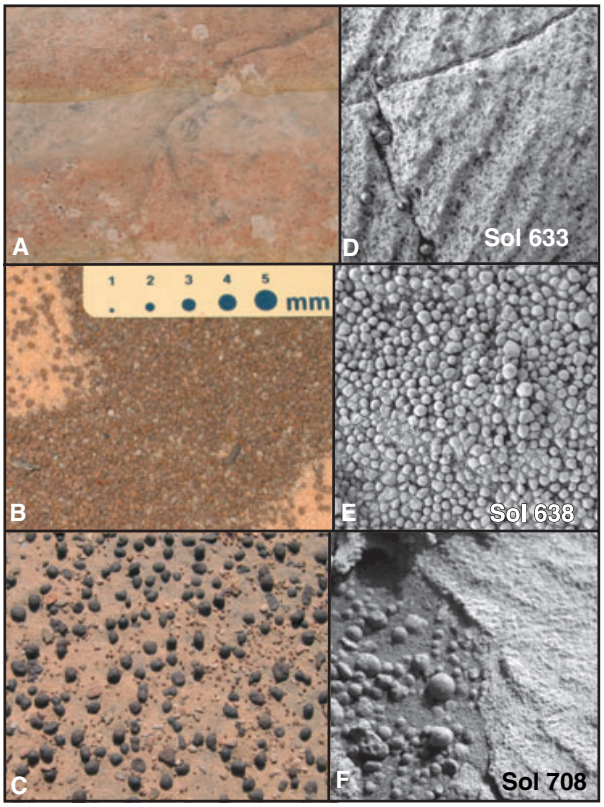

Fig. 6. Comparative and similar examples of terrestrial Navajo Sandstone at left with Mars 'berries' at right Micro Imager pictures on the right (D,E,F) are approximately 3 cm across (Image credits: NASA/JPL/Cornell). Tiny (1 mm-size) concretions both insitu (A in red banded reaction front) and in accumulations (B) from the Navajo Sandstone are comparable to 'microberries' (~1 mm diameter in D-E) in the Burns formation, Meridiani Planum. Two populations of accumulated weathered loose Navajo concretions (C) show larger dark colored 0.8 mm–1.2 cm diameter 'marbles' and smaller 1mm or smaller brown colored 'mini concretions'. These two terrestrial populations show similarities to the 'blueberries' and 'microberries' on Mars (F) where larger berries are ~4.2 mm in diameter.

here, both varieties of concretions (Fig. 6) suggest varying diffusive and advective mass-transfer rates and concentrations of iron in the water.

Some modern acid saline lakes in Western Australia (Benison & Bowen 2006) contain evaporite mineralogies that may be chemically similar to the sulfate mineralogy of the Mars system (e.g. Tosca *et al.* 2005; McLennan *et al.* 2005), and iron mobilization geochemistry of Meridiani Planum was likely under acidic conditions (e.g. Fernández-Remolar *et al.* 2004). Despite different chemical systems, the spectacular exposure and variability of Navajo concretions (geometries and compositions) reveal spatial distributions that help provide a working model to interpret Mars 'microberries' and 'blueberries'. The numerical experiments suggest that acidic conditions would allow Fe^{2+} to stay in solution so that the Mars spherules could develop at some distance from the iron source. Iron may be derived from the weathering of basalts that are subjected to highly acidic water, and 'blueberry' precipitations may occur where the water is less acidic. The laboratory bench tests presented here also suggest that the Mars hematite precipitates can be further modified through diffusion-driven re-mineralization as the host sediment's pore water property and other physical conditions (such as temperature and saturation) change.

Although it is difficult to find terrestrial analogs for Mars in every respect, analog differences and variations can add breadth and depth to the understanding and interpretation of new planetary data. Our experiments do not intend to simulate the exact chemistry of either the Utah or the Meridiani environment. However, they can elucidate the physical process of concretion growth, which may have applications to both terrestrial and Martian examples.

CONCLUSIONS

Jurassic Navajo Sandstone examples of very small (<1 cm-scale) and 'mini' (mm-scale) spherical iron-oxide concretions are common and are expected as a result of redox reactions. Field observations and numerical simulations indicate that spherical iron oxide concretions can form in a variety of host-rock conditions. Furthermore, numerical simulations show cross-diffusion of solutes in homogeneous sediments can produce patterned hematite precipitates (banding or concretions). It is also evident that advective fluid flow (in combination with diffusion) is important to the development of widespread concretions. Laboratory tests indicate that chemical gradients between the inside and the outside of these spheres cause diffusion of Fe ions toward the outer perimeter of the amorphous sphere, forming a rind. The rind then grows inwards due to diffusion within the sphere, and may produce 'onion layering'. Continued diffusion, dehydration, or changing temperature are a few of the factors that may further affect the secondary internal structure-forming processes.

The occurrence of specular gray hematite 'blueberries' at Meridiani Planum (Herkenhoff *et al.* 2004; Squyres *et al.* 2004) suggests varying conditions of diffusion with supersaturated solutions and temperature/pressure regimes that favored the formation of hematite (with or without intermediate iron oxide stages), as well as an abundant and reactive iron source. Open diagenetic systems may have a number of complicating factors operating over long periods of geologic time, and aspects of the nucleation warrant further investigation.

ACKNOWLEDGEMENTS

We gratefully acknowledge Peter Mozley and an anonymous reviewer for their constructive comments to help improve this manuscript. This publication is based upon

work supported by the National Aeronautics and Space Administration under Grant Number NNG06GI10G (to M. Chan) issued through the Mars Fundamental Research Program. The work by J. Ormö was supported by the Spanish Ministry for Science and Education (References AYA2003-01203 and CGL2004-03215/BTE). J. Ormö and V. Souza-Egipsy were supported by the Spanish Ramón y Cajal Program. M. Stich was supported by the Spanish Instituto Nacional de Técnica Aeroespacial. G. Komatsu was supported by the Italian Space Agency.

SUPPLEMENTARY MATERIAL

The following supplementary material is available for this article:

Appendix S1. Water-rock interaction numerical model (Word document). This material is available as part of the online article from: http://www.blackwell-synergy.com/doi/abs/10.1111/j.1468-8123.2007.00187.x (This link will take you to the article abstract).

Please note: Blackwell Publishing are not responsible for the content or functionality of any supplementary materials supplied by the authors. Any queries (other than missing material) should be directed to the corresponding author for the article.

REFERENCES

Atkinson K (1988) *An Introduction to Numerical Analysis*. John Wiley & Sons, New York, 693 pp.

Beitler B, Parry WT, Chan MA (2003) Bleaching of Jurassic Navajo Sandstone on Colorado Plateau Laramide highs: evidence of exhumed hydrocarbon supergiants? *Geology*, **31**, 1041–4.

Beitler B, Parry WT, Chan MA (2005) Fingerprints of fluid flow: chemical diagenetic history of the Jurassic Navajo Sandstone, southern Utah, USA. *Journal of Sedimentary Research*, **75**, 545–59.

Benison KC & Bowen BB (2006) Acid saline lake systems give clues about past environments and the search for life on Mars. *Icarus*, **183**, 225–9.

Berner RA (1968) Rate of concretion growth. *Geochimica et Cosmochimica Acta*, **32**, 477–83.

Berner RA (1969) Goethite stability and the origin of red beds. *Geochimica et Cosmochimica Acta*, **33**, 267–73.

Berner RA (1980) *Early Diagenesis: A Theoretical Approach*. Princeton University Press, Princeton, NJ.

Borkow PS & Babcock LE (2003) Turning pyrite concretions outside-in: role of biofilms in pyritization of fossils. *The Sedimentary Record*, **1**, 4–7.

Boudreau B (1996) *Diagenetic Models and their Implementation*. Springer, New York, 414 pp.

Chan, MA, Parry WT, Bowman JR (2000) Diagenetic hematite and manganese oxides and fault-related fluid flow in Jurassic sandstones, southeastern Utah. *American Association of Petroleum Geologists Bulletin*, **84**, 1281–310.

Chan MA, Parry WT, Petersen EU, Hall CM (2001) ^{40}Ar–^{39}Ar age and chemistry of manganese mineralization in the Moab to Lisbon fault systems, southeastern Utah. *Geology*, **29**, 331–4.

Chan MA, Beitler B, Parry WT, Ormö J, Komatsu G (2004) A possible terrestrial analogue for hematite concretions on Mars. *Nature*, **429**, 731–4.

Chan MA, Beitler BB, Parry WT, Ormö J, Komatsu G (2005) Red rock and red planet diagenesis: comparisons of Earth and Mars concretions. *Geological Society of America Today*, **15**, 4–10.

Chan MA, Johnson CM, Beard BL, Bowman JR, Parry WT (2006) Iron isotopes constrain the pathways and formation mechanisms of terrestrial oxide concretions: a tool for tracing iron cycling on Mars? *Geosphere*, **2**, 324–32.

Christensen PR, Wyatt MB, Glotch TD, Rogers AD, Anwar S, Arvidson RE, Bandfield JL, Blany DL, Budney C, Calvin WM, Fallacaro A, Fergason RL, Gorelick N, Graff TG, Hamilton VE, Hayes AG, Johnson JR, Knudson AT, McSween HY Jr., Mehall GL, Mahall LK, Moersch JE, Morris RV, Smith MD, Squyres SW, Ruff SW, Wolff MJ (2004) Mineralogy at Meridiani Planum from the mini-TES experiment on the Opportunity Rover. *Science*, **306**, 1733–9.

Cornell RM, Schwertmann U (2003) *The Iron Oxides: Structure, Properties, Reactions, Occurrences, and Uses*, 2nd edn. Wiley-VCH Publishers, New York, NY, 703 pp.

Crank J (1979) *The Mathematics of Diffusion*, 2nd edn. Clarendon Press, Oxford, 406 pp.

Fernández-Remolar D, Gomez-Elvira J, Gomez F, Sebastian E, Martin J, Manfredi JA, Torres J, Gonzalez Kesler C, Amils R (2004) The Tinto River, an extreme acidic environment under control of iron, as an analog of the Terra Meridiani hematite site of Mars. *Planetary Space Science*, **53**, 239–48.

Flicker M, Ross J (1974) Mechanism of chemical instability for periodic precipitation phenomena. *Journal of Chemical Physics*, **60**, 3458–65.

Fu L, Milliken KL, Sharp JM Jr. (1994) Porosity and permeability variations in the fractured and liesegang-banded Breathitt Sandstone (Middle Pennsylvanian), eastern Kentucky: diagenetic controls and implications for modeling dual porosity systems. *Journal of Hydrology*, **154**, 351–81.

Grotzinger JP, Bell JF III, Calvin W, Clark BC, Fike DA, Golombek M, Greeley R, Herkenhoff KE, Jolliff B, Knoll AH, Malin M, McLennan SM, Parker T, Soderblom L, Sohl-Dickstein JN, Squyres SW, Tosca NJ, Watters WA (2005) Stratigraphy, sedimentology and depositional environment of the Burns Formation, Meridiani Planum, Mars. *Earth and Planetary Science Letters*, **240**, 11–72.

Hall JS, Mozley PS, Davis JM, Delude-Roy N (2004) Environments of formation and controls on spatial distribution of calcite cementation in Plio-Pleistocene fluvial deposits, New Mexico, USA. *Journal of Sedimentary Research*, **74**, 643–53.

Henisch HK (2005) *Crystals in Gels and Liesegang Rings*. Cambridge University Press, Cambridge, 212 pp.

Herkenhoff KE, Squyres SW, Arvidson R, Bass DS, Bell JF III, Bertelse P, Cabrol NA, Gaddis L, Hayes AG, Hviid SF, Johnson JR, Kinch KM, Madsen MB, Maki JN, McLennan SM, McSween HY Jr., Rice JW Jr., Sims M, Smith PH, Soderblom LA, Spanovich N, Sullivan R, Wang A (2004) Evidence from Opportunity's microscopic imager for water on Meridiani Planum. *Science*, **306**, 1727–30.

Klein, JS, Mozley P, Campbell A, Cole R (1999) Spatial distribution of carbon and oxygen isotopes in laterally extensive carbonate-cemented layers; implications for mode of growth and subsurface identification. *Journal Sedimentary Research*, **69**, 184–91.

McLennan SM, Bell JF III, Calvin W, Christensen PR, Clark BC, de Souza PA, Farmer J, Farrand WH, Fike DA, Gellert R, Ghosh A, Glotch TD, Grotzinger JP, Hahn B, Herkenhoff KE, Hurowitz JA, Johnson JR, Johnson SS, Jolliff BL, Klingelhöfer G, Knoll AH, Learner ZA, Malin MC, McSween HY Jr., Pocock J, Ruff SW, Soderblom LA, Squyres SW, Tosca NJ, Watters WA, Wyatt MB, Yen A (2005) Provenance and diagenesis of the evaporite-bearing Burns formation, Meridiani Planum, Mars. *Earth and Planetary Science Letters*, **240**, 95–121.

Morris RV, Ming DW, Graff TG, Arvidson RE, Bell JF III, Squyres SW, Mertzman SA, Gruener JE, Golden DC, Le L, Robinson GA (2005) Hematite spherules in basaltic tephra altered under aqueous, acid sulfate conditions on Mauna Kea volcano, Hawaii: possible clues for the occurrence of hematite-rich spherules in the Burns formation at Meridiani Planum, Mars. *Earth and Planetary Science Letters*, **240**, 168–78.

Mozley PS (1989) Complex compositional zonation in concretionary siderite: implications for geochemical studies. *Journal of Sedimentary Petrology*, **59**, 815–8.

Mozley PS (1996) The internal structure of carbonate concretions: a critical evaluation of the concentric model of concretion growth. *Sedimentary Geology*, **103**, 85–91. doi:10.1016/0037-0738(95)00087-9.

Mozley PS (2003) Diagenetic structures. In: *Encyclopedia of Sediments and Sedimentary Rocks* (ed. Middleton G), pp. 219–25. Kluwer Academic Press, Dordrecht.

Mozley PS & Davis JM (2005) Internal structure and mode of growth of elongate calcite concretions: evidence for small-scale, microbially induced, chemical heterogeneity in groundwater. *Geological Society of America Bulletin*, **117**, 1400–12. doi: 10.1130/B25618.1.

Müller SC, Ross J (2003) Spatial structure formation in precipitation reactions. *Journal of Physical Chemistry A*, **107**, 7997–8008.

Ormö J, Komatsu G, Chan MA, Beitler B & Parry WT (2004) Geological features indicative of processes related to the hematite formation in Meridiani Planum and Aram Chaos, Mars: a comparison with diagenetic hematite deposits in southern Utah, USA. *Icarus*, **171**, 295–316. doi: 10.1016/j.icarus.2004.06.001.

Ortoleva PJ (1984) The self organization of Liesegang bands and other precipitate patterns. In: *Chemical Instabilities, Applications in Chemistry, Engineering, Geology, and Materials Science* (eds Nicolis G, Baras F), pp. 289–97. NATO ASI series C, D. Reidel Publishing Co., Dordrecht-Boston.

Ortoleva PJ (1994) *Geochemical Self-Organization.* Oxford University Press, Oxford, 411 pp.

Park AJ, Ortoleva PJ (2003) Multi-mineralic water–rock interaction, mass-transfer and textural dynamics simulator. *Computers and Geosciences*, **29**, 277–90.

Park AJ, Chan MA, Parry WT (2005) Water–rock interaction simulations of iron oxide mobilization and precipitation: implications of cross-diffusion reactions for terrestrial and Mars 'blueberry' hematite concretions. *EOS Transactions American Geophysical Union*, **86**, Fall Meeting Supplement Abstract P21A-0138.

Parry WT, Chan MA, Beitler B (2004) Chemical bleaching indicates fluid flow in sandstone deformation bands. *American Association of Petroleum Geologists Bulletin*, **88**, 175–91.

Press, W (1992) *Numerical Recipe in C: the Art of Scientific Computing*, 2nd edn. Cambridge University Press, Cambridge, 994 pp.

Raiswell R, Fisher QJ (2000) Mudrock-hosted carbonate concretions: a review of growth mechanisms and their influence on chemical and isotopic composition. *Journal of the Geological Society*, **157**, 239–51.

Roussel CJ, Roussel MR (2004) Reaction–diffusion models of development with state-dependent chemical diffusion coefficients. *Progress in Biophysics & Molecular Biology*, **86**, 113–60.

Schwertmann R & Cornell RM (2000) *Iron Oxides in the Laboratory. Preparation and Characterization*, 2nd edn. Wiley-VCH Publishers, New York.

Schwertmann U, Stanjek H, & Becher H-H, (2004) Long-term in vitro transformation of 2-line ferrihydrite to goethite/hematite at 4, 10, 15 and 25°C. *Clay Minerals*, **39**, 433–8; doi: 10.1180/0009855043940145.

Scott SK & Showalter K (1992) Simple and complex propagating reaction-diffusion fronts. *Journal of Physical Chemistry*, **96**, 8702–11.

Seilacher A (2001) Concretion morphologies reflecting diagenetic and epigenetic pathways. *Sedimentary Geology*, **143**, 41–57.

Sjoberg EL, Rickard DT (1984) The influence of experimental design on the rate of calcite dissolution,. *Geochimica et Cosmochimica Acta*, **47**, 2281–5.

Souza-Egipsy V, Ormö J, Bowen BB, Chan MA, Komatsu G (2006) Ultrastructural study of iron oxide precipitates: implications for the search for biosignatures in the Meridiani hematite concretions, Mars. *Astrobiology*, **6**, 527–45.

Squyres SW (2005) Sagan lecture: spirit, opportunity, and the exploration of the red planet. *EOS Transactions American Geophysical Union*, **86**, Fall Meeting Supplement Abstract P11D-01.

Squyres SW, Knoll AH (2005) Sedimentary rocks at Meridiani Planum: Origin, diagenesis, and implications for life on Mars. *Earth and Planetary Science Letters*, **240,** 1–10.

Squyres SW, Grotzinger JP, Arvidson RE, Bell JF III, Calvin W, Christensen PR, Clark BC, Crisp JA, Farrand WH, Kerkenhoff KE, Johnson JR, Klingelhofer G, Knoll AH, McLennan SM, McSween HY Jr., Morris RV, Rice JW , Rieder R, Soderblom LA (2004) In situ evidence for an ancient aqueous environment at Meridiani Planum, Mars. *Science*, **306**, 1709–14.

Stumm W, Morgan J (1996) *Aquatic Chemistry: Chemical equilibria and rats in natural waters.* 3rd edn. John Wiley & Sons, New York, pp. 1040.

Thorson JP, MacIntyre TJ (2005) Geology of the Cashin Mine sandstone-hosted disseminated copper deposit, Montrose County, Colorado. *Society of Economic Geologists Guidebook*, **37**, 43–49 (digital only).

Tosca NJ, McLennan SM, Clark BC, Grotzinger JP, Hurowitz JA, Knoll AH, Schröder C, Squyres SW (2005) Geochemical modeling of evaporation processes on Mars: insight from the sedimentary record at Meridiani Planum. *Earth and Planetary Science Letters*, **240**, 122–48.

Walker TR (1967) Formation of red beds in modern and ancient deserts. *Geological Society of America Bulletin*, **78**, 353–68.

Walker TR (1975) Red beds in the western interior of the United States. *U.S. Geological Survey Professional Paper*, **853**, 49–56.

Williamson MA, Rimstidt JD (1994) The kinetics and electrochemical rate-determining step of aqueous pyrite oxidation. *Geochimica et Cosmochimica Acta*, **24**, 543–5454.

Wolery T, Jackson K, Bourcier W, Bruton C, Viani C, Knauss K, Delany J (1990) *Current Status of the EQ3/6 Software Package for Geochemical Modeling.* American Chemical Society Symposium Series 416. American Chemical Society, Washington, DC, 104–16.